Journal of

Applied and Computational Mechanics

Shahid Chamran
University of Ahvaz

Journal of Applied and Computational Mechanics

Higher-Order Slope Limiters for Euler Equation

Arun Govind Neelan[1] , Manoj T. Nair[2]

[1] Department of Aerospace Engineering, Indian Institute of Space Science and Technology-Thiruvananthapuram,
Valiyamala, Thiruvananthapuram, 695547, India, arunneelaniist@gmail.com

[2] Department of Aerospace Engineering, Indian Institute of Space Science and Technology-Thiruvananthapuram,
Valiyamala, Thiruvananthapuram, 695547, India, manojtnair@iist.ac.in

Abstract. High-resolution schemes are designed for resolving shocks without significant numerical dissipation and dispersion. Achieving higher-order and high-resolution is a challenging task because of the non-monotonicity of the higher-order schemes. In this article, we have presented second-order and third-order slope limiters having an improved shock resolution and accuracy. The present limiters are tested on one-dimensional and two-dimensional unstructured grids and compared with the existing limiters. The numerical result shows that the present limiters have an excellent shock resolving property and accuracy than other limiters. In blast wave problems, it has shown over 200% more accurate results than the other limiters.

Keywords: Finite volume method, high-resolution method, higher-order methods, slope-limiter.

1. Introduction

Lightweight structures are commonly used in aerospace applications for greater performance and efficiency. The safety factor (FOS) used in airframes is less than 1.4 [1] to reduce the overall weight. Due to the lightweight and low FOS, an accurate estimate of the load is essential for aircraft design. Airframes are generally subject to thermal and mechanical loading. These loads are highly sensitive to Mach number, pressure and temperature. These loads increase exponentially with Mach number. Small inaccuracy in estimating the Mach number may lead to an inefficient design or failure of aircraft due to loads. We need a very accurate numerical scheme to precisely solve the shock and other parameters that affect the load. In this work, we have proposed a scheme that is more accurate than other numerical schemes for shock resolution and other key parameters such as pressure, temperature, velocity, etc.

Euler equations are the most common form of equations that describe the adiabatic, inviscid, compressible flow. These equations represent the Cauchy equations of the conservation of mass, momentum and energy, which constitute a set of coupled nonlinear differential equations. It is relatively complicated to obtain an analytical solution for this equation. The complex delta shock structure for the isentropic relativistic Chaplygin-Euler equations can be found in [2, 3]. The complete analytical solution of the Euler equation is very complicated, and there is no general solution for all kinds of initial and boundary conditions. The Euler equation with initial conditions that are piecewise constant is generally referred to as the Riemann problem. They lead to some complex wave phenomena, such as shock waves, expansion waves, shock-shock interactions, blast waves, etc. These complex structures arise from the interaction of nonlinear acoustic waves present in the Euler equation. Various test cases are proposed to study these waves in the literature, and a commonly used test case is the shock-tube problem. The shock tube is one of the experimental devices used to study the flow properties in the supersonic and hypersonic flows.

The numerical solution of the Euler equation using piecewise parabolic [4] approach with high-resolution property is presented. The Finite Volume Method (FVM) discretization with high-resolution framework significantly improved the ability to resolve shocks in high-speed flows. The accuracy of FVM depends mainly on the discretization stencil, the Riemann solver, and the quality of the grid. Popular approaches commonly used in the reconstruction of the left and the right state are flux-limiters and weighted essentially non-oscillatory (WENO) schemes [5, 6]. The flux-limiters are widely used in Computational Fluid Dynamics (CFD) because of their robustness, accuracy and higher stability compared to other high-resolution schemes [7]. The flux-limiters are based on the concept of total variation diminishing (TVD), that is, they will not allow the solution to explode by bounding its value. TVD schemes are relativity less accurate at extrema, and they may give diffused result at shocks.

The reduction in the order of accuracy of the shock TVD schemes is intended to maintain monotony [8]. The basics of these limiters can be found in [9, 10]. The classical Monotone Upstream-Central Scheme for Conservation Laws (MUSCL) scheme is a second-order scheme that is extended to third-order [11]. A fourth-order polynomial reconstruction with monotony preserving properties is presented in [12]. Parabolic reconstructions are subject to Runge's phenomena, so hyperbolic reconstitution is explored in [13]. All the second-order conservative discretization schemes can be expressed in a general form - such schemes are called κ-schemes [14].

$$\mathbf{U}_{i+0.5} = \frac{1}{2}(\mathbf{U}_{i+1} + \mathbf{U}_i) - \frac{1-\kappa}{4}(\mathbf{U}_{i+1} - 2\mathbf{U}_i + \mathbf{U}_{i-1}) \tag{1}$$

Equation (1) can be viewed as a central difference scheme with the addition of an artificial dissipation term. Without an artificial dissipation term, schemes become unstable when combined with an explicit Euler time integration. Thus, all higher-order schemes use bias that leads to numerical dissipation. This biasing is required to provide upwinding for hyperbolic equations [15]. Equation (1) will reduce to different schemes for different values of κ. For example, it will be reduced to the linear-upwind scheme [16] for $\kappa = -1$. Equation (1) becomes the Fromm scheme [17] for $\kappa = 0$ because the dispersion term in truncation error disappears at that value. Cubic-upwind interpolation [18] scheme is recovered for $\kappa = 1/3$. The quadratic-upwind interpolation scheme [19] can be obtained by substituting $\kappa = 1/2$ in eq. (1). For $\kappa = 1$ central difference scheme is obtained. A comparison of the performance of different limiters is presented in [7, 14].

Minmod limiter [20] is relatively more diffusive but can handle poor quality mesh and a variety of flow conditions. Superbee limiter [21] was proposed to improve the shock-resolving properties of the limiter. Due to the aggressive switching nature of superb, the solution may produce oscillations. To make a compromise between resolution and dispersion, a limiter that is smoothly varying in the Sweby diagram [10] is proposed in [22]. A popular limiter that does not fall into the monotone region of the Sweby diagram for the negative values of r is introduced in [23]. CHARM [24] is a limiter in which flux limiter value can go up to three. This maximum value of flux-limiter can be viewed as an anti-diffusion term for slope correction in the face flux calculation. This value cannot be increased arbitrarily because it can lead to unphysical oscillations in the solution. Minmod limiter with sign preserving property can be found in [25].

Other popular flux-limiters are Koren limiter [26], Chakravarthy limiter [27], OSPRE [28], SMART [29], UMIST [30]. Most of the TVD schemes that ensure monotonicity in one-dimension may not work well on multi-dimensional problems [31], and it can be even worse on unstructured grids. To overcome this, a multi-dimensional unstructured edge-based limiter is presented in [31]. An efficient high-resolution relaxation scheme for hyperbolic conservation law systems is explored in [32]. Second-order TVD schemes with added artificial viscosity are studied in [33]. A unified, universal total variation stability region and a new flux-limiter are proposed in [34].

In this paper, a second-order and a third-order limiter having high accuracy and high shock resolving property are proposed and compared with the existing limiters. The limiters are tested on one-dimensional and two-dimensional test cases and found improvement over other limiters considered in this work. The following test cases are studied in the present work.

1. Shock tube problem: This is a critical test case in the solution of compressible flow equations, as the exact time-dependent solution is known for some initial conditions. The initial solution to this problem is made up of two uniform states separated by a discontinuity at the origin. This initial value problem is known as the Riemann problem. In experiments, this initial solution represents a tube with left and right regions separated by a diaphragm and filled with the same gas in two different thermodynamic states. When the diaphragm bursts, the discontinuity between the two initial states breaks into moving waves to the left and the right, separated by a contact surface. The wave pattern consists of a contact discontinuity in the middle and a shock or expansion wave on either side. Different initial states give moving discontinuities of different strengths and speeds, making this an excellent test case for numerical schemes. Figure 1 (a) shows a schematic of the problem.

2. Flow past a supersonic wedge: When the supersonic flow encounters a corner, the flow is turned into itself and compressed. At the turn, an oblique shock is produced. An exact solution to this problem is available, and applications include the supersonic aircraft engine intakes and the wings of the supersonic aircraft. The strength of the shock and angle changes with the wedge angle and inflow Mach number. Figure 1 (b) shows a schematic of the problem.

3. Flow past a wedge with the shoulder: This test case has an inward turning of flow due to a wedge followed by an outward turning of the flow, at the shoulder. The results in an oblique shock at the inward turning and expansion fans at the shoulder. This test case is relevant to supersonic intakes and a sharp nose of supersonic configurations. Exact solutions for different angles of the wedge are available once again. Figure 1 (c) shows a schematic of the problem.

4. Blast wave problem: The Woodward-Colella interacting blast wave problem consists of an initial solution with a low-pressure region is placed between two high-pressure regions on either side. These types of problems are observed in volcanic eruptions, oceanic blasts, the explosion of explosives, etc. This test case results in the interaction between the shock wave, contact wave, and rarefaction wave. Figure 1 (d) shows a schematic of the problem.
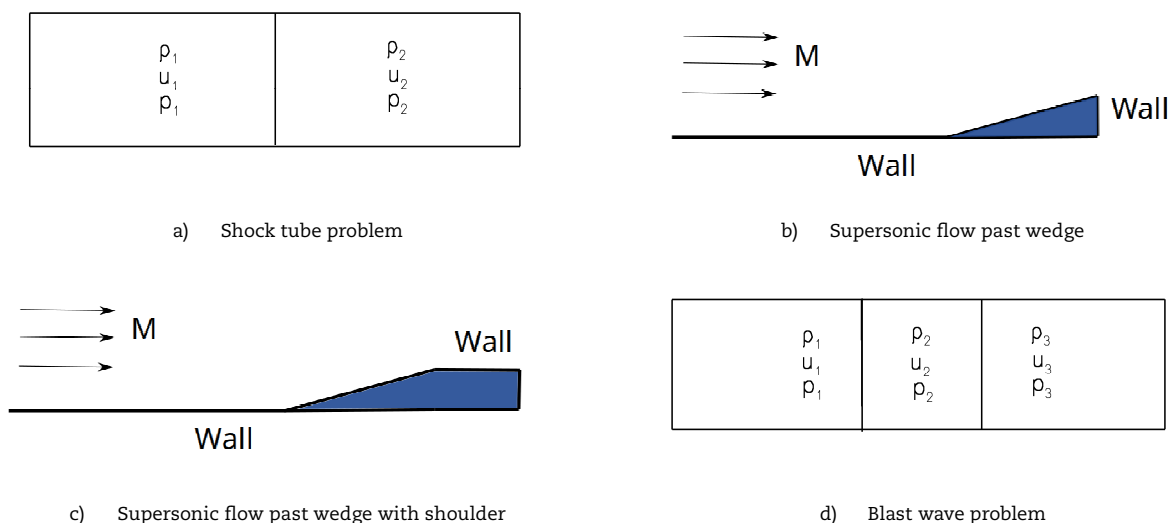

a)   Shock tube problem

b)   Supersonic flow past wedge

c)   Supersonic flow past wedge with shoulder

d)   Blast wave problem

Fig. 1. Test cases for the Euler equation

2. Governing Equation and Discretization

The governing differential equation considered in this work is Euler equation. One-dimensional Euler equation is

$$\frac{\partial \mathbf{U}}{\partial t} + \frac{\partial \mathbf{F}}{\partial x} = 0 \tag{2}$$

$$\mathbf{U} = \begin{bmatrix} \rho \\ \rho u \\ \rho e_t \end{bmatrix} \quad \mathbf{F} = \begin{bmatrix} \rho u \\ \rho u^2 + p \\ u(\rho e_t + p) \end{bmatrix} \tag{3}$$

Formulating weak form of the equation by doing volume averaging in the cell $I_i \equiv [i-0.5, i+0.5]$ using the method of line leads to

$$\frac{d\overline{\mathbf{U}}_i}{dt} = -\frac{1}{\Delta x}(\mathbf{F}_{i+0.5} - \mathbf{F}_{i-0.5}) \tag{4}$$

where $\mathbf{F}_{i+0.5}$ is numerical flux at the cell face computed from $\mathbf{F}_{i+0.5} = \mathbf{F}(\mathbf{U}^R_{i+0.5}, \mathbf{U}^L_{i+0.5})$ and $\mathbf{U} \in \mathrm{R}^3$. The second-order numerical flux may be achieved by evaluating $\mathbf{U}^R_{i+0.5}$, $\mathbf{U}^L_{i+0.5}$ given in eq. (5), but it may end up in oscillations in the non-smooth data because of non-monotonicity.

$$\mathbf{U}^L_{i+0.5} = \mathbf{U}_i + \frac{\Delta x}{2}d\mathbf{U} + \frac{\Delta x^2}{8}d^2\mathbf{U}$$

$$\mathbf{U}^R_{i+0.5} = \mathbf{U}_{i+1} - \frac{\Delta x}{2}d\mathbf{U} + \frac{\Delta x^2}{8}d^2\mathbf{U} \tag{5}$$

We should limit the gradients, as given in eq. (6).

$$\mathbf{U}^L_{i+0.5} = \mathbf{U}_i + \frac{\Delta x}{2}L[d\mathbf{U}] + \frac{\Delta x^2}{8}L[d^2\mathbf{U}]$$

$$\mathbf{U}^R_{i+0.5} = \mathbf{U}_{i+1} - \frac{\Delta x}{2}L[d\mathbf{U}] + \frac{\Delta x^2}{8}L[d^2\mathbf{U}] \tag{6}$$

where L is the limiter operator. Unlike the incompressible flow, one cannot directly calculate $\mathbf{U}^L_{i+0.5}$ or $\mathbf{U}^R_{i+0.5}$ because of the presence of shocks in the compressible flow. Limiting the value of $d\mathbf{U}$ and $d^2\mathbf{U}$ using slope-limiter should be carried out, else this will create non-physical oscillations in the solution. The left and right states are calculated by Monotonic Upwind Scheme for Conservation Laws (MUSCL) approach using the limiters proposed here. Because the Roe scheme violated entropy condition, Harten entropy fix [35] based on the jump present in the conserved variable is employed. For time integration, the hyperbolic Runge-Kutta method [36] is used.

2.1 Discretization of FVM on unstructured mesh

Integrating the Euler equation over the control volume Ω along the boundary Γ and applying Green-Gauss divergence theorem,

$$\frac{\partial}{\partial t}\iint_\Omega \mathbf{U}\, d\Omega + \oint_\Gamma (\mathbf{F}.\vec{n})d\Gamma = 0 \tag{7}$$

where $\vec{n}$ is unit normal vector at edge of control volume. For 2-D it can be written as [37]

$$\frac{d\mathbf{U}}{\partial t} = -\frac{1}{|\Omega_p|}\sum_i (\mathbf{F_x}.\overrightarrow{n_x} + \mathbf{F_y}.\overrightarrow{n_y})\delta\Gamma_i \tag{8}$$

where Σ_p is a the cell, $\Sigma_p \subset \Sigma$ and Γ_i is the edge and $\Gamma_i \subset \Gamma$. $\mathbf{F_x}$ and $\mathbf{F_y}$ are x and y components of the flux. The Jacobian of flux is

$$A_n = \frac{\partial \mathbf{F}}{\partial \mathbf{U}} = \begin{bmatrix} 0 & \mathbf{n_t} & 0 \\ (\gamma-1)\frac{q^2}{2}\mathbf{n} - q_n\mathbf{v} & \mathbf{v}\otimes\mathbf{n} + (1-\gamma)\mathbf{n}\otimes\mathbf{v} + q_n I & (\gamma-1)\mathbf{n} \\ \left(\frac{\gamma-1}{2}q^2 - H\right)q_n & H\mathbf{n_t} - (1-\gamma)\mathbf{v^T}q_n & q_n \end{bmatrix} \tag{9}$$

where $\mathbf{q_n} = un_x + vn_y$, $\mathbf{n_t} = \begin{bmatrix} 1 & 0 \end{bmatrix}^T$, $\mathbf{v} = \begin{bmatrix} u & v \end{bmatrix}$. I is identity matrix of size 2×2.

3. Second-order Slope Limiter

In this section, a second-order limiter is presented and the numerical properties of these limiters are discussed. Second-order flux-limiters are commonly used in CFD, but obtaining a high-resolution solution without significant wiggles is always a challenging task using an aggressive limiter. In this section, a computationally economical the second-order limiter is presented. Second-order limiter used here is similar to the form presented in [14]. The representation and implementation of the limiter used in the present work slightly differ from flux-limiters in [10]. The interpolation scheme can be written as

$$\mathbf{U}_{i+0.5} = \mathbf{U}_i + \frac{\Delta x}{2} L[\partial \mathbf{U}(\mathbf{U}^+, \mathbf{U}^-))] \tag{10}$$

where $L[\partial \mathbf{U}] = \psi(r)\partial \mathbf{U}(\mathbf{U}^+, \mathbf{U}^-)$, $\psi(r)$ is the limiter function, $r = \mathbf{U}_1^- / \mathbf{U}_1^+$, $\mathbf{U}_1^+ = \mathbf{U}_{i+1} - \mathbf{U}_i$ and $\mathbf{U}_1^- = \mathbf{U}_i - \mathbf{U}_{i-1}$.

3.1 MMF1

This limiter is a modification of the minmod limiter. Here, a different approach is used to choose the limiting parameter.

$$L[\partial \mathbf{U}(\mathbf{U}^+, \mathbf{U}^-)] = \begin{cases} \mathbf{U}_1^+ + c(\mathbf{U}_1^- - \mathbf{U}_1^+)abs\left(\dfrac{\mathbf{U}_1^+}{\mathbf{U}_1^- + \epsilon}\right)\psi, & \text{if} \quad abs(\mathbf{U}_1^+) < abs(\mathbf{U}_1^-) \\[3mm] \mathbf{U}_1^- + c(\mathbf{U}_1^+ - \mathbf{U}_1^-)abs\left(\dfrac{\mathbf{U}_1^-}{\mathbf{U}_1^+ + \epsilon}\right)\psi, & \text{if} \quad abs(\mathbf{U}_1^+) \geq abs(\mathbf{U}_1^-) \end{cases} \tag{11}$$

where $\psi = \text{abs}([\text{sign}(\mathbf{U}_1^-) + \text{sign}(\mathbf{U}_1^+)] / 2)$, $c = 1$ and $\varepsilon = 10^{-9}$.

As the classical minmod chooses the absolute minimum of the slopes between right and left slopes, for a second-order scheme it diffuses the result. If the highest slope is chosen, it gives oscillations. To reduce dissipation, a small anti-diffusion term is added to the slope obtained from minmod. The resultant slope value is in-between the original highest and lowest value. The magnitude of anti-diffusion is controlled by the r such that the limiter stays in the monotone region. Regardless of the value of r , the present limiter always lies in the monotone region.

4. Third Order Slope-limiters

A third-order TVD limiter is presented where the first and second derivative in the interpolation of the left and right fluxes have been limited. The general third-order scheme to calculate face value at $i + 0.5$ is

$$\mathbf{U}_{i+0.5}^L = \mathbf{U}_i + \frac{\Delta x}{2} L[\partial \mathbf{U}(\mathbf{U}^+, \mathbf{U}^-, \mathbf{U}^0)] + \frac{\Delta x^2}{8} L[\partial^2 \mathbf{U}]$$

$$\mathbf{U}_{i+0.5}^R = \mathbf{U}_{i+1} - \frac{\Delta x}{2} L[\partial \mathbf{U}] + \frac{\Delta x^2}{8} L[\partial^2 \mathbf{U}(\mathbf{U}^+, \mathbf{U}^-, \mathbf{U}^0)] \tag{12}$$

where L is the limiter operator which operates on the gradients. In the stencil, $[i-2, \ i+2]$ there are three ways to calculate $\partial^2 \mathbf{U}$ and they are

$$\begin{aligned} \mathbf{U}_2^- &= \mathbf{U}_{j-2} - 2\mathbf{U}_{j-1} + \mathbf{U}_j & \mathcal{O}(\Delta x) \\ \mathbf{U}_2^0 &= \mathbf{U}_{j-1} - 2\mathbf{U}_j + \mathbf{U}_{j+1} & \mathcal{O}(\Delta x^2) \\ \mathbf{U}_2^+ &= \mathbf{U}_j - 2\mathbf{U}_{j+1} + \mathbf{U}_{j+2} & \mathcal{O}(\Delta x) \end{aligned} \tag{13}$$

4.1 Minmod_s2

Equation (6) gives the three possible second gradient calculation expressions for the stencil $[i-2, \ i+2]$. The safest choice is to choose the minimum among $|\mathbf{U}_2^+|$, $|\mathbf{U}_2^-|$ and $|\mathbf{U}_2^0|$. The minmod_s2 limiter is:

$$L[\partial^2 \mathbf{U}(\mathbf{U}_2^+, \mathbf{U}_2^-, \mathbf{U}_2^0)] = \begin{cases} \mathbf{U}_2^+ \psi, & \text{if } abs(\mathbf{U}_2)^+ < abs(\mathbf{U}_2^-) & \text{and} \quad abs(\mathbf{U}_2^+) < abs(\mathbf{U}_2^0) \\ \mathbf{U}_2^- \psi, & \text{if } abs(\mathbf{U}_2^-) \geq abs(\mathbf{U}_2^-) & \text{and} \quad abs(\mathbf{U}_2^0) \geq abs(\mathbf{U}_2^-) \\ \mathbf{U}_2^0 \psi & \text{else} \end{cases} \tag{14}$$

where $\psi = (\text{sign}(\mathbf{U}_2^+) + \text{sign}(\mathbf{U}_2^-)) / 2$.

This limiter is similar to convex-ENO (C-ENO) proposed in [38]. However, they have used limiters on $\mathbf{U}_2^-$ and $\mathbf{U}_2^0$, but not on $\mathbf{U}_2^+$. In the present limiter, extra conditions are implemented to improve the stability and accuracy of the scheme, but the limiter is computationally expensive than C-ENO. C-ENO and the present scheme are compared for Shu-Osher problem. The initial condition used for this problem is:

$$(\rho, u, p) = \begin{cases} (3.857143, 2.629369, 10.33333) & x \leq -4 \\ (1 + 0.2 \times sin(5x), 0, 1) & x > -4 \end{cases} \tag{15}$$

Figure 2 shows the solution of Shu-Osher problem with 400 grid points at flow time 1.8 s. The problem is solved using Courant-Friedrichs-Lewy (CFL) number 0.8. CFL is defined as $CFL = (abs(u) + a)\Delta t / \Delta x$, u where is velocity of flow, a speed of sound. The reference solution is obtained using minmod limiter with 2000 grid points. C-ENO produced oscillations when high CFL number is used. When CFL number is less than 0.7, C-ENO did not produce any oscillations on this grid. The various combinations of first and second-order term treatment used is listed in the Table 1.

5. Results of the Second-order Limiter

In this section, the behavior of MMF1 limiter on different standard test cases for 1-D and 2-D Euler equations are studied. The performance of the present limiters on the unstructured triangular grid is also evaluated.

5.1 Sod shock tube problem

The initial conditions for the problem are

$$(\rho, u, p) = \begin{cases} (1, 0, 1) & x \leq 0.5 \\ (0.125, 0, 0.1) & x > 0.5 \end{cases} \tag{16}$$

Table 1. List of the reconstruction schemes used.

Notation	1st derivative	2nd derivative
MMF1	MMF1	-
Cada [39]	Cada	-
MM-S2	minmod	minmod_s2
MMF1-S2	MMF1	minmod_s2
Convex-ENO [38]	minmod	Minmod

Table 2. L_2 error in Sod shock tube problem using different limiters.

Limiters	E_ρ	E_u	E_p	% E_ρ
Minmod	0.029949108	0.097347997	0.034681065	125.7823
Superbee	0.023958118	0.087255857	0.026877834	100.6209
Van Albada	0.028097104	0.093829356	0.032254258	118.0041
MMF1	0.023810274	0.079651239	0.026100415	100

This problem is solved using 200 grid points with $CFL = 0.5$. A second-order four-stage hyperbolic Runge-Kutta method (HRK42) [36] is used for time integration. Interpolation is carried out in the primitive variables using the MUSCL scheme using different limiters. Standard Roe scheme with entropy fix as used for Riemann solver. A comparison of various limiters with MMF1 is presented in Fig. 3. From the figure, it is clear that MMF1 has better discontinuity resolving capability than all the limiters considered in this paper. The result of MMF1 is comparable to the superb limiter. L_2 error of the solution with different limiters is shown in Table 2.

The error is calculated using eq. (17).

$$E_\rho = \sqrt{\left(\frac{\sum_{i=1}^{i=n} (\rho_i^{exact} - \rho_i^{numerical})^2}{n^2} \right)} \tag{17}$$

The relative error % E_ρ is calculated using eq. (18).

$$\%E_\rho = \frac{E_\rho^{lim\,iter}}{E_\rho^{MMF1}} \times 100 \tag{18}$$

In eq. (18), E_ρ^{MMF1} is root mean square (RMS) error of MMF1. $E_\rho^{lim\,iter}$ is the RMS error of other limiters. In this test case, MMF1 is more accurate than other limiters. The result of superb and MMF1 is more or less the same, but MMF1 is more accurate than superb in velocity (Table 2). The present limiter is 25% more accurate than minmod limiter.
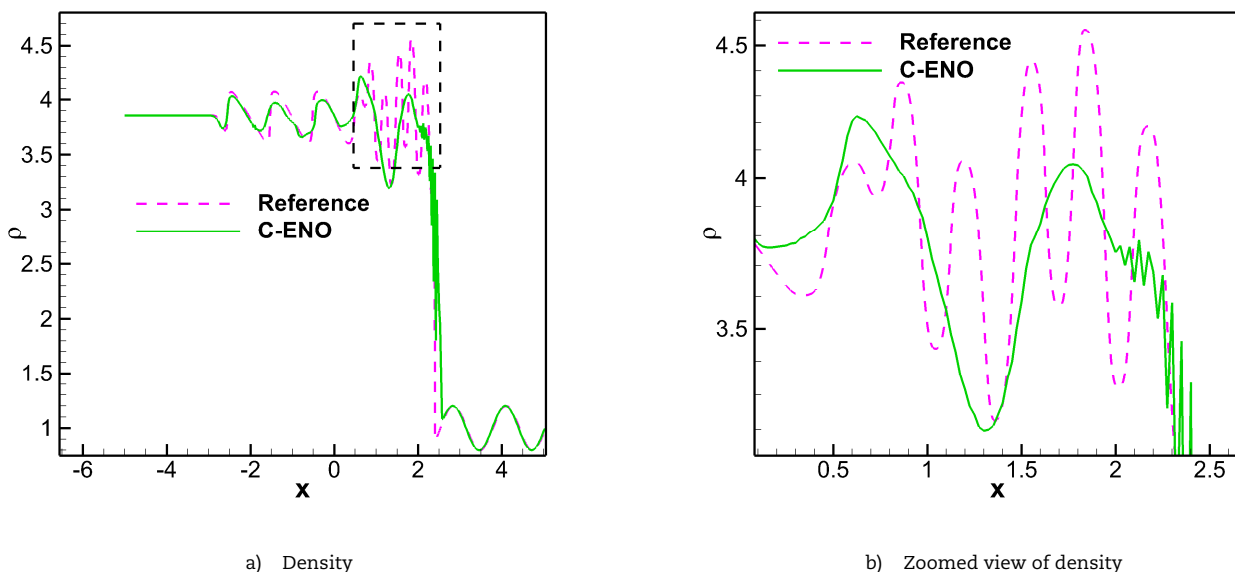

a) Density

b) Zoomed view of density

Fig. 2. Density plot of Shu-Osher problem with 400 grid points with $CFL = 0.8$.

Table 3. L_2 error in right expansion and left strong shock problem using different limiters.

Limiters	$\mathbf{E}_\rho$	$\mathbf{E_u}$	$\mathbf{E_p}$	% $\mathbf{E}_\rho$
Minmod	0.0345567	0.0876217	0.2968190	106.6815
Superbee	0.0315612	0.0870069	0.2947563	97.434
Van Albada	0.0336739	0.0878657	0.2977279	103.9563
MMF1	0.0323924	0.0867438	0.2942133	100

5.2 Right expansion and left strong shock

This case has a pressure jump in the initial condition, and other variables do not have any jumps. The initial conditions used are

$$(\rho, u, p) = \begin{cases} (1,0,7) & x \le 0.5 \\ (1,0,10) & x > 0.5 \end{cases} \tag{19}$$

The numerical simulation is carried out using 200 grid points with $CFL = 0.9$. The solution is obtained up to flow time of T = 0.1 s and the results are shown in Fig. 4. L_2 error of this test case is presented in Table 3. The performances of all the limiters are similar, but superb has a lower density error. MMF1 is better than others in velocity and pressure fields. In general, MMF1 limiter is more accurate than superb limiter on a coarse grid and superb limiter is more accurate on a finer grid.

a)   Density

b)   Zoomed view of discontinuity

c)   Zoomed view of discontinuity

d)   Zoomed view of discontinuity
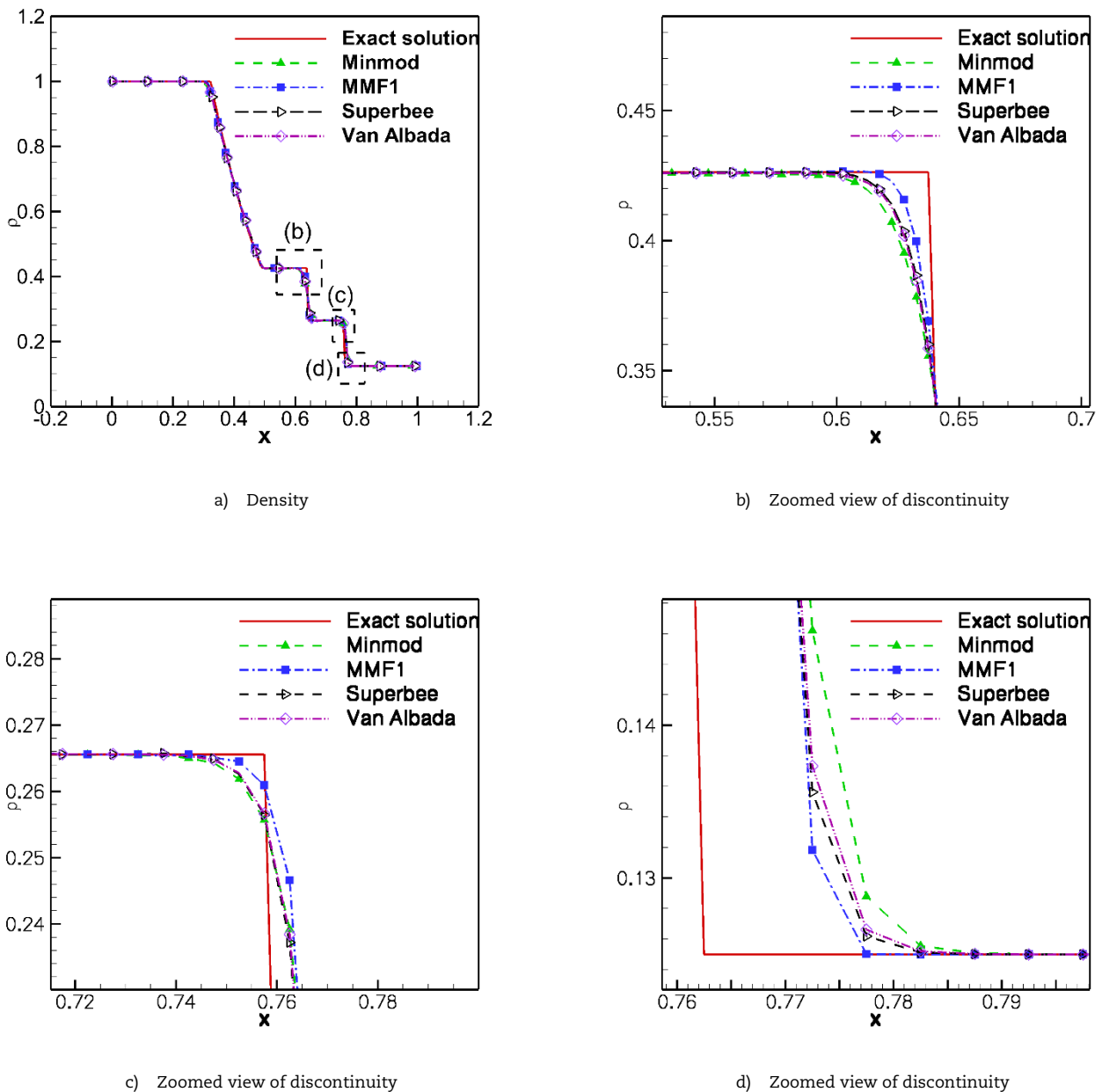
Fig. 3. Density plot of Sod shock tube problem with 200 grid points with $CFL = 0.5$ at $t = 0.15$.

Table 4. L_2 error in in Mach number 3 problem using different limiters.

Limiters	E_ρ	E_u	E_p	% E_ρ
Minmod	0.081226	0.073182	0.234189	137.6793
Superbee	0.060195	0.039913	0.154488	102.0321
Van Albada	0.073034	0.063915	0.202328	123.7938
MMF1	0.058996	0.057073	0.170774	100

a)   Density

b)   Zoomed view of discontinuity

c)   Zoomed view of discontinuity

d)   Zoomed view of discontinuity
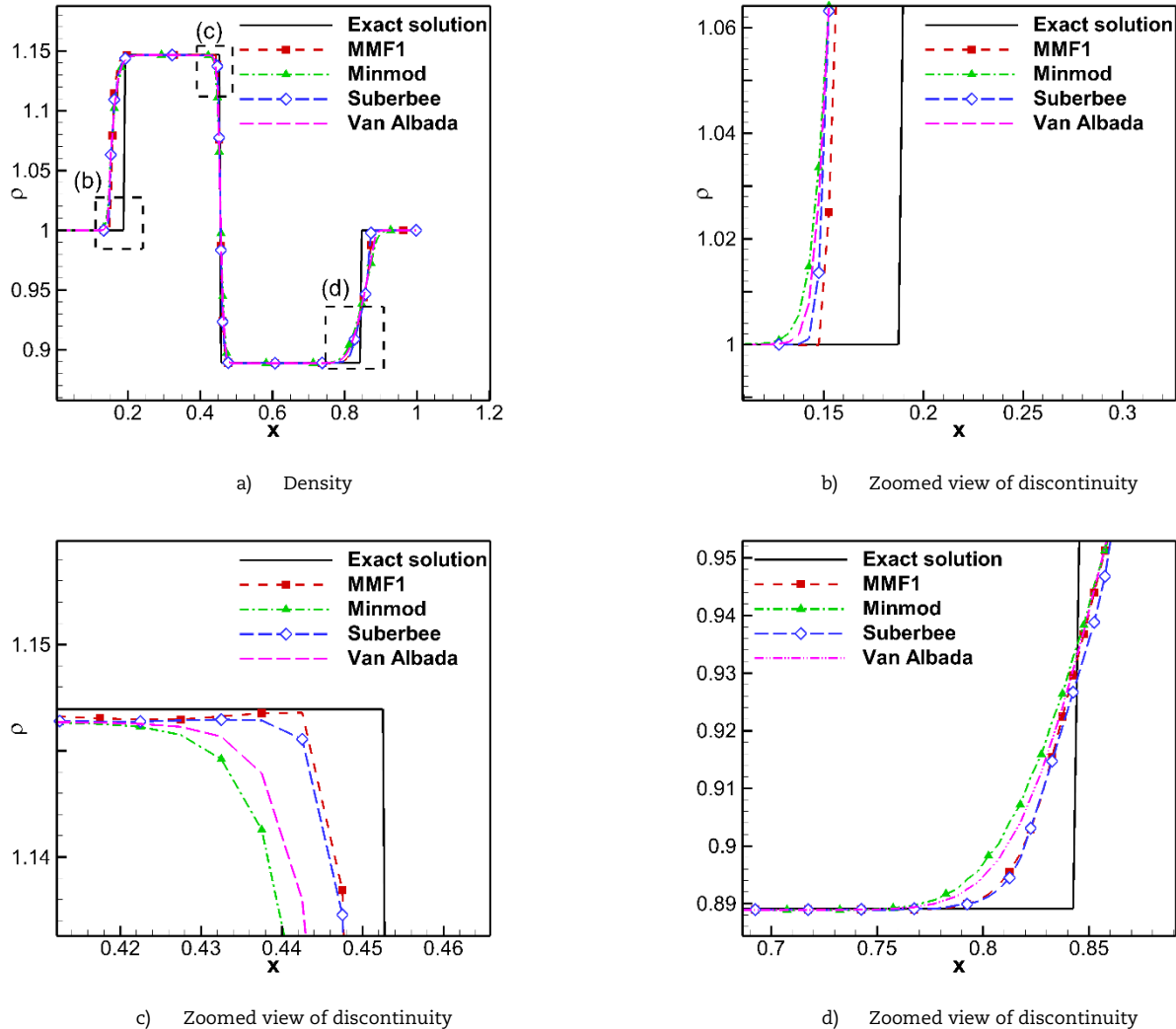
Fig. 4. Density plot of Right Expansion and left strong shock tube problem with 200 grids *CFL*=0.9 at 0.1 s

5.3 Mach number 3 test case

The initial conditions used are:

$$(\rho, u, p) = \begin{cases} (3.857, 0.92, 10.333) & x \leq 0.5 \\ (1, 3.55, 1) & x > 0.5 \end{cases} \tag{20}$$

The problem is solved using 200 grid points with $CFL = 0.9$. The problem is simulated up to flow time of 0.09 s and the results are shown in Fig. 5. For this problem, MMF1 limiter outperformed other limiters. The RMS error of this test case is tabulated in Table 4. MMF1 limiter is 37% more accurate than minmod limiter.

5.4 Supersonic flow over a wedge

Supersonic flow at Mach number 6.5 over 10^0 wedge is solved. The problem is solved using a 401×401 quadrilateral grid. The boundary condition used a slip wall on the wedge and free stream condition at other boundaries. The gradients are limited using MMF1 limiter. Time integration is carried using implicit Euler method. The Mach number contour is shown in Fig. 6. There is no significant variation in the solution between MMF1 and minmod, but the resolution of MMF1 is better than minmod and superb as shown in Fig. 7.

Root mean square (RMS) error of minmod and MMF1 are 0.106882 and 0.097375 respectiv1ely. In terms of RMS error, MMF1 is 9.7% more accurate than minmod. For this configuration, in the pressure load estimation of wing design, MMF1 limiter can save up to 5 newtons per square meter than minmod limiter. For a standard fighter aircraft, it can save up to 500 N, which is more than two times the war-head of Asthira missile of India.
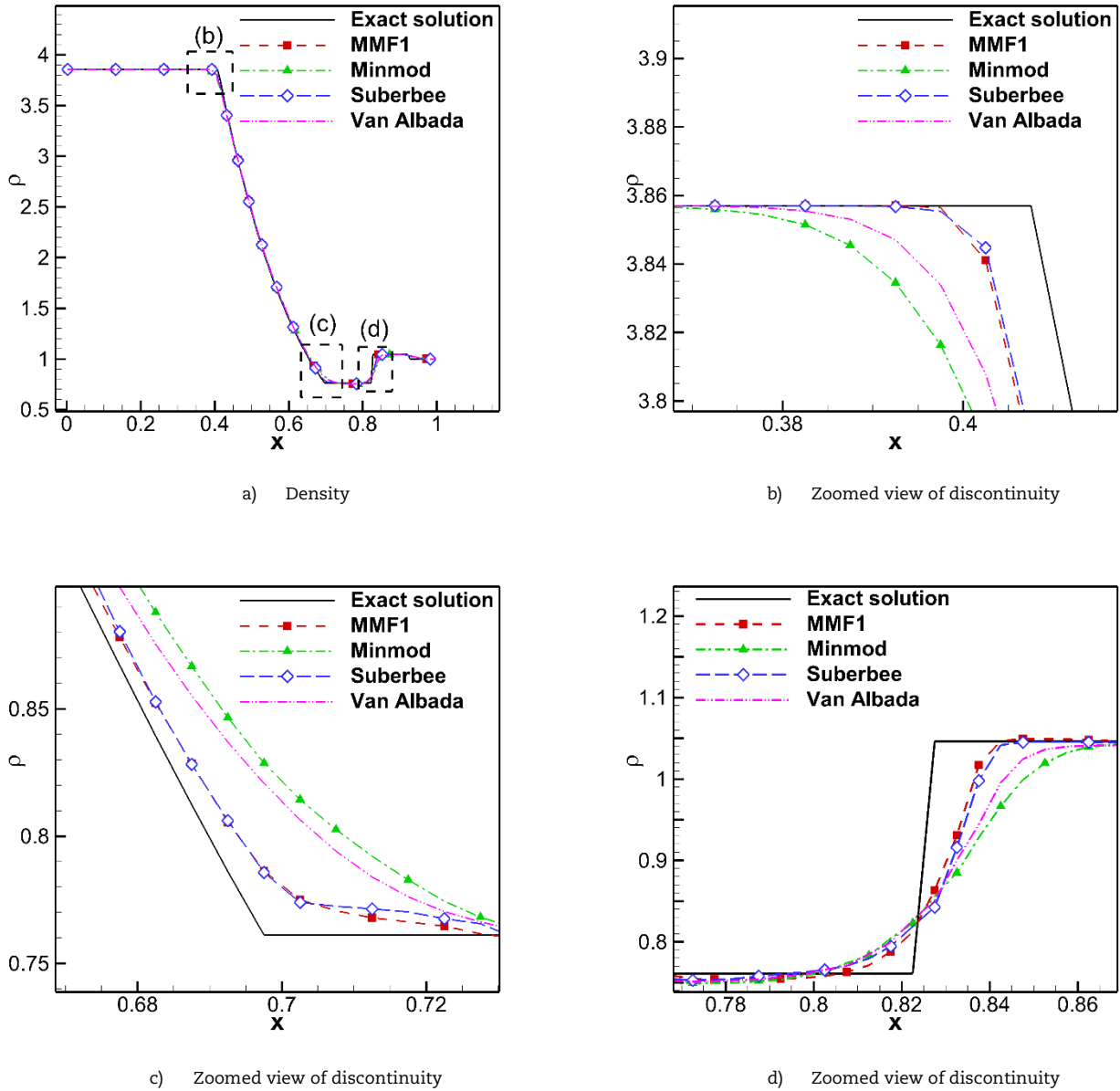
a)   Density

b)   Zoomed view of discontinuity

c)   Zoomed view of discontinuity

d)   Zoomed view of discontinuity

Fig. 5. Density plot of Mach = 3 test with 200 grids *CFL* = 0.9 at T= 0.09s
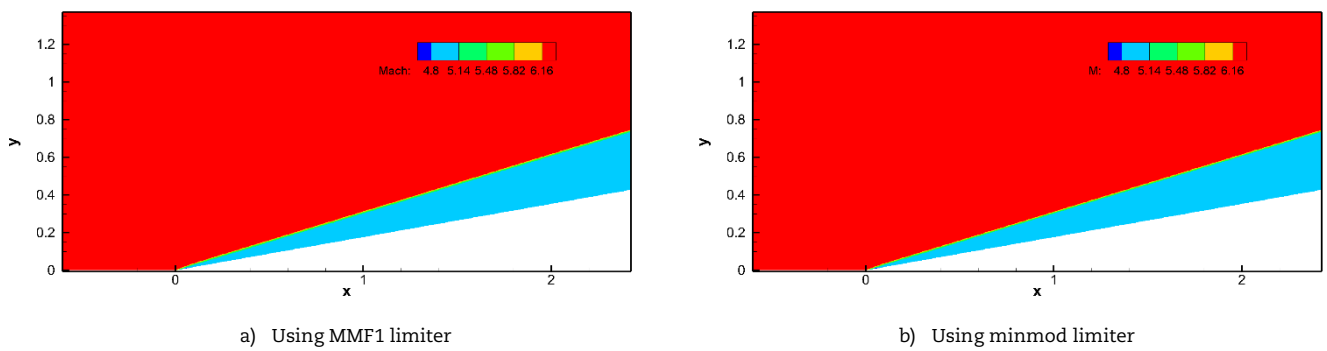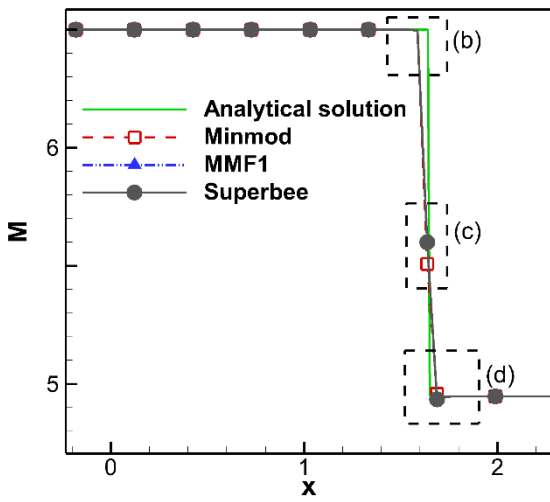

a)   Using MMF1 limiter
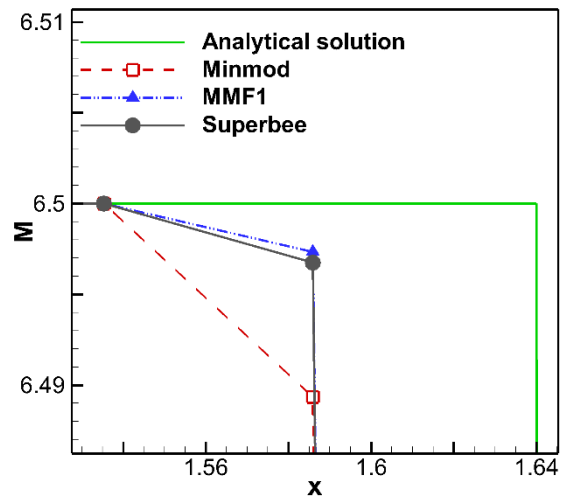

b)   Using minmod limiter

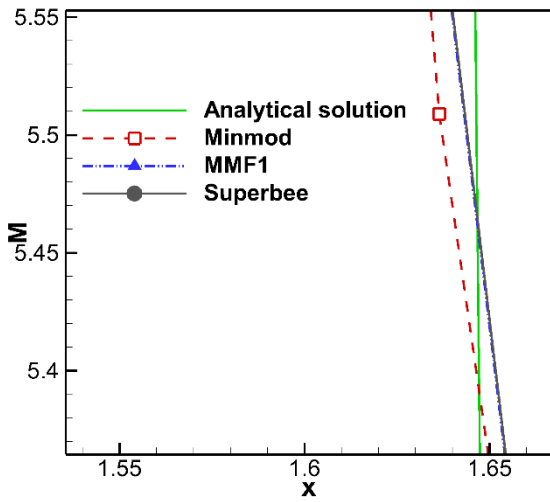**Fig. 6.** Supersonic flow past 10^0 wedge with M = 6.5

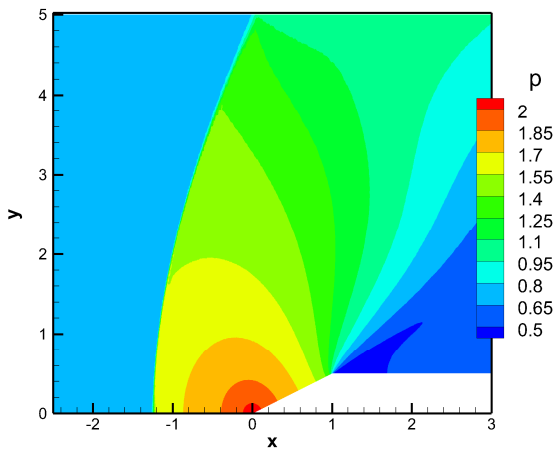a)   Variation of Mach number at y = 0.5

b)   Zoomed view of discontinuity

c)   Zoomed view of discontinuity
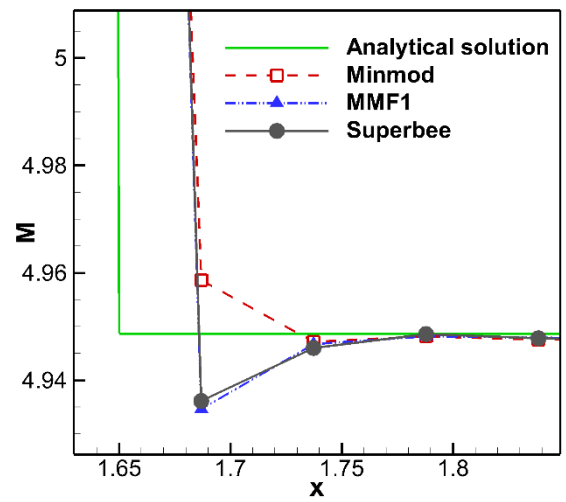
d)   Zoomed view of discontinuity

Fig. 7. Supersonic flow past 10° wedge with M = 6.5

a)   Pressure contour of the wedge
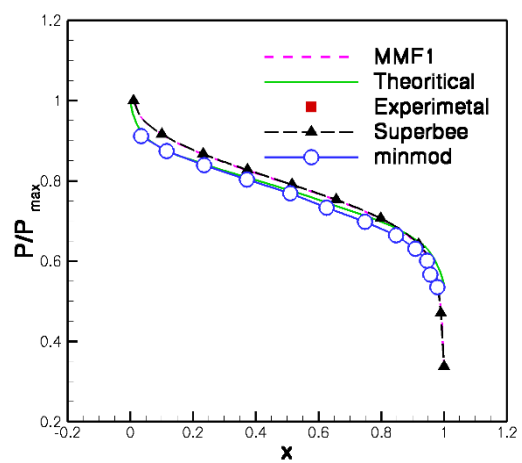
b)   Pressure on the surface of the wedge

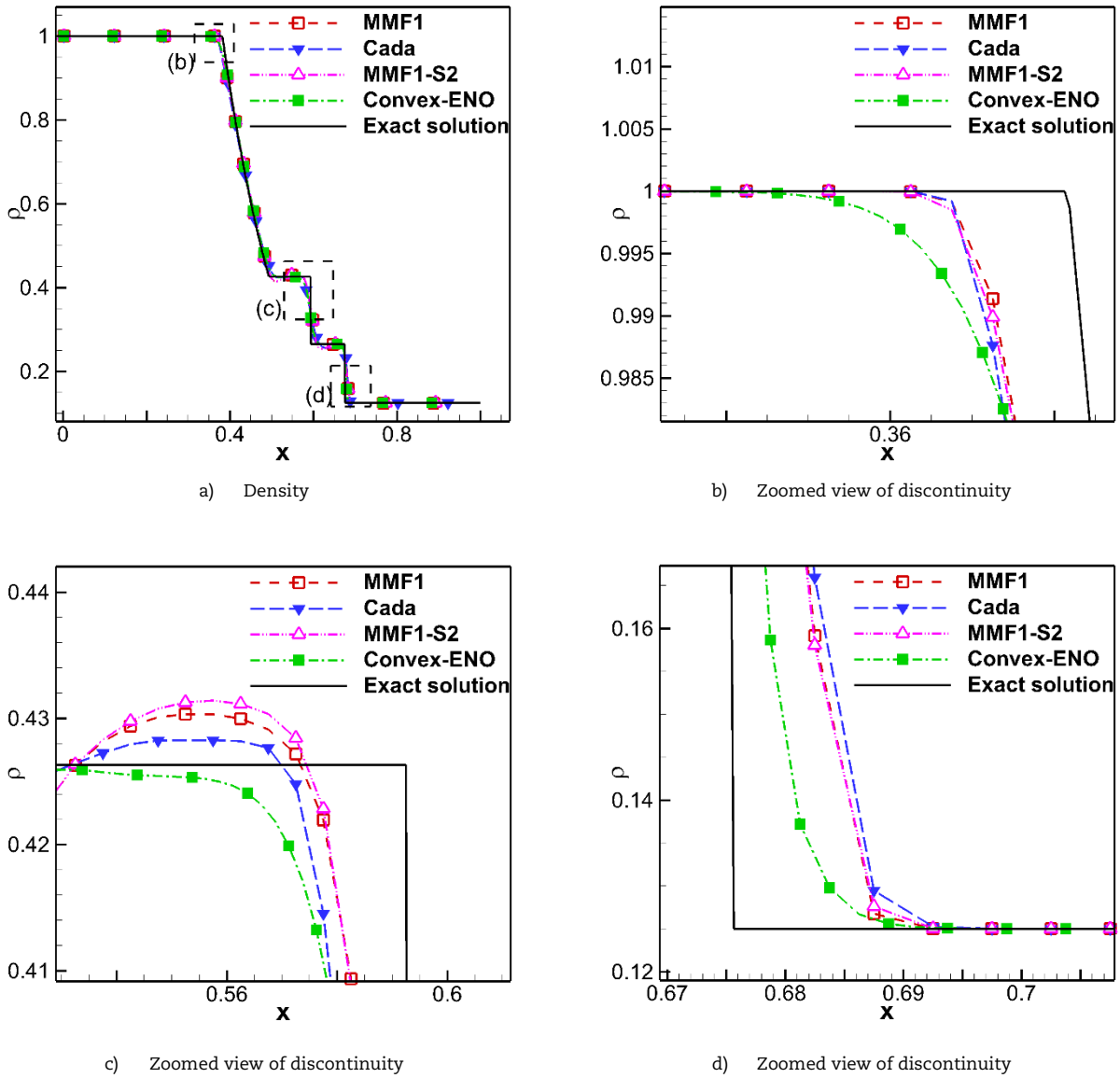**Fig. 8.** Supersonic flow past 10° wedge with M = 6.5

a)   Density

b)   Zoomed view of discontinuity

c)   Zoomed view of discontinuity

d)   Zoomed view of discontinuity

Fig. 9. Density plot of Sod shock tube problem using 400 grids CFL = 0.5 at T = 0.1 s

Table 5. L_2 error in Sod shock tube problem.

Limiters	E_ρ	E_u	E_p	% E_ρ
MMF1	0.012085929	0.055583416	0.012893991	100
CADA	0.014126912	0.059664611	0.014680221	116.8873
MM-S2	0.015526093	0.059992679	0.015825881	128.4642
MMF1-S2	0.012049288	0.054684266	0.012724591	99.6968
Convex-ENO	0.01010391	0.03618296	0.0090118	83.6006

Table 6. L_2 error of Shu-Osher problem.

Limiters	E_ρ	E_u	E_p	% E_ρ
MMF1	0.121069366	0.047402636	0.190404816	100
Cada	0.094859715	0.022425722	0.094337962	78.3515
MM-S2	0.091178647	0.020078345	0.09260607	75.3111
MMF1-S2	0.078841668	0.021502648	0.094778111	65.1211
Convex-ENO	0.11988841	0.04358392	0.18415129	99.0246

Table 7. L_2 error in Blast wave interaction test case.

Limiters	E_ρ	E_u	E_p	% E_ρ
MMF1	0.07925544	21.44495695	21.7792556	100
Cada	0.19745523	21.40694564	30.2437603	249.1378
MM-S2	0.33655261	21.37375978	38.0867291	424.6429
MMF1-S2	0.07987625	21.44441891	18.9531758	100.7833
Convex-ENO	0.3359265	21.3678743	39.063563	423.8529

a)   Density

b)   Zoomed view of discontinuity

c)   Zoomed view of discontinuity

d)   Zoomed view of discontinuity
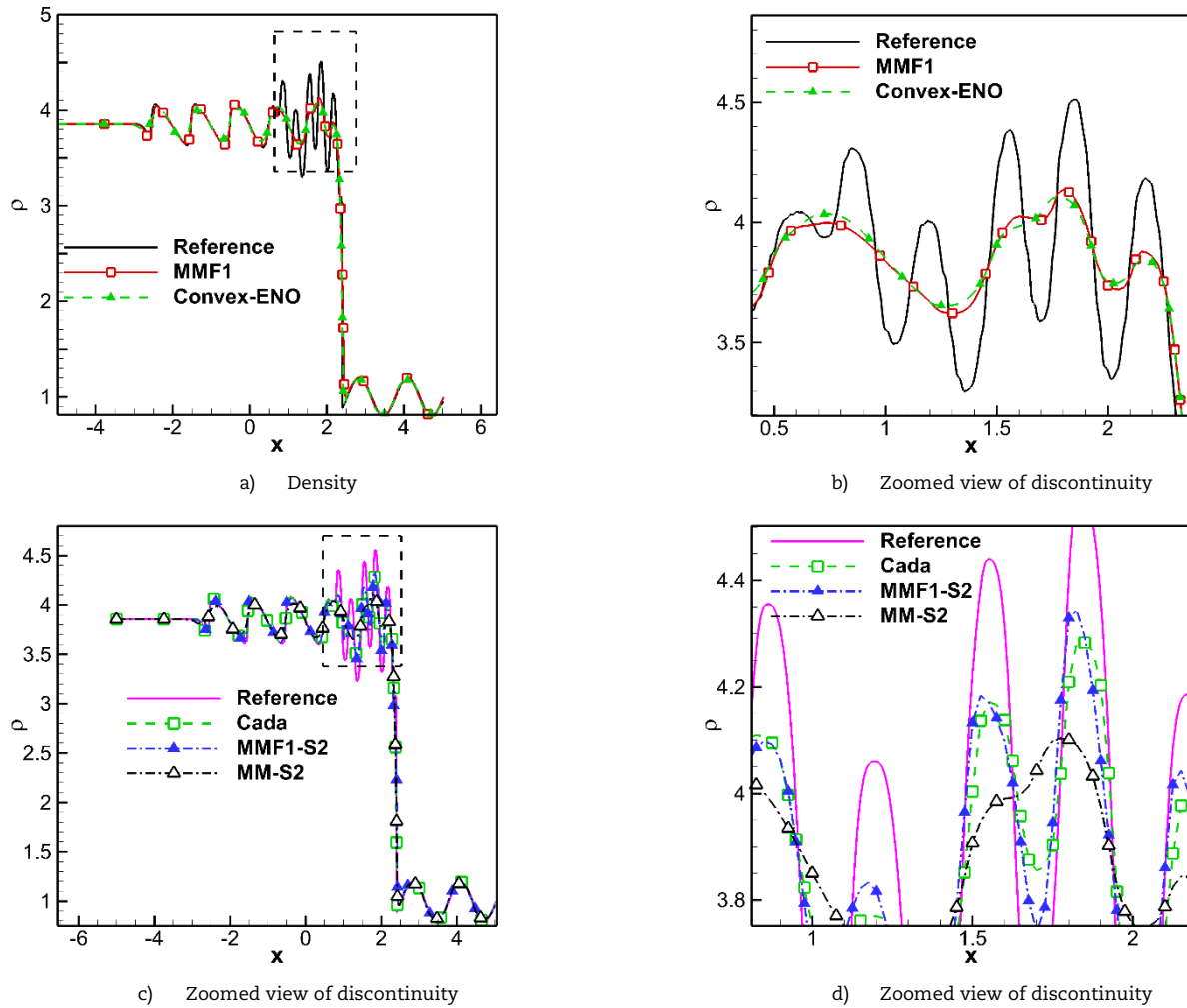
Fig. 10. Comparison of limiters on Shu-Osher problem.

a)   Density

b)   Zoomed view of density

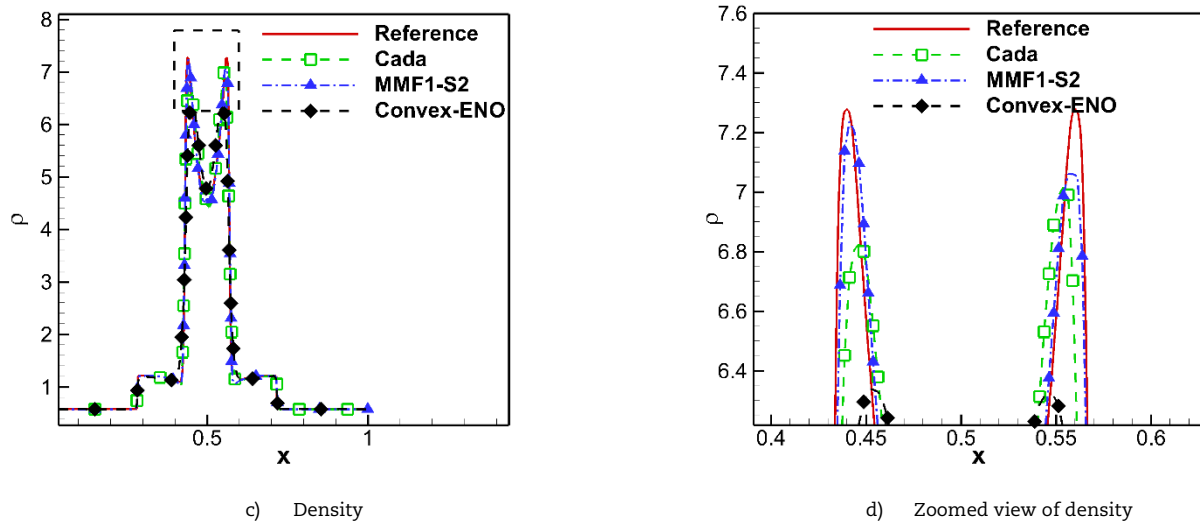c)   Density

d)   Zoomed view of density
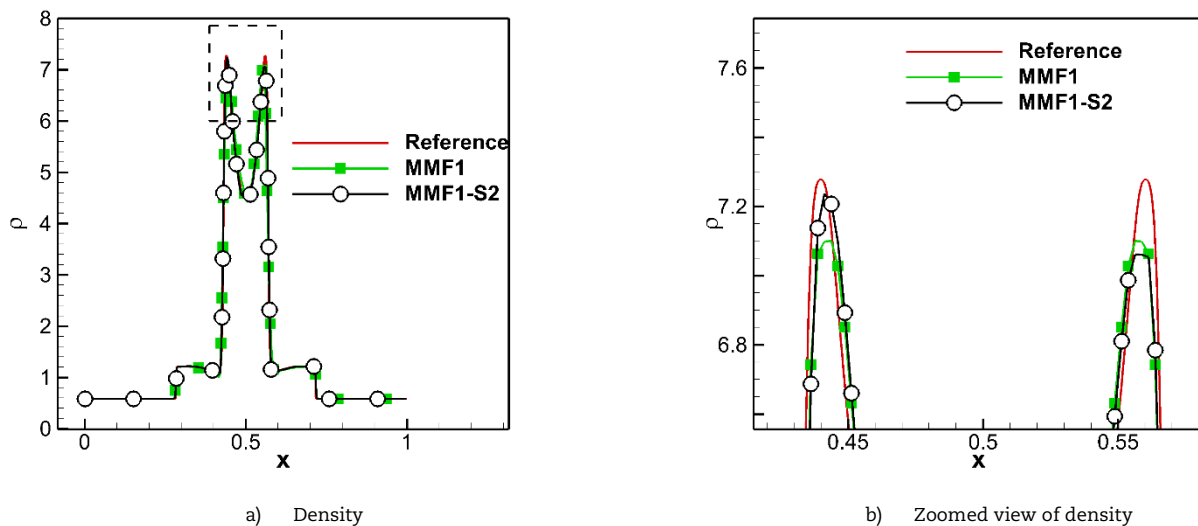
Fig. 11. Density plot of blast wave interaction at T = 0.025 s

5.5 Supersonic flow over a wedge with expansion fan

To ensure the capability of the present limiter on the unstructured grid, the limiter is tested on a wedge with turning angle of 26.6° followed by a shoulder. The simulation is carried on a 500×200 grid at a free stream Mach (M) number 1.44. The boundary conditions are zero normal velocity on the lower boundary (wall), and free-stream condition at other boundaries. Moving least square with Gaussian kernel is used for interpolation. Time integration is carried out using the implicit Euler method. The vertex-centered scheme is more accurate than the cell-centered scheme for isotopic mesh so the vertex-centered scheme is used. Here, an unstructured triangle grid is generated and edge-based limiting procedure is followed. The pressure contours for the test case are shown in Fig. 8a. The comparison of the experimental [40] and the theoretical result with the computational result is shown in Fig. 8b.

6. Results of the Third-order Limiter

In this section, the results of the third-order limiters are presented. The results of third-order limiters are better than the second-order limiters. In general, third-order limiter works well for problems having curvatures.

6.1 Sod shock tube problem

Sod shock tube problem is solved using 200 grid points using CFL = 0.5. The test case is solved up to flow time 0.1 s. The initial condition is given in eq. (16). The density plot of the test case is shown in Fig. 9. From the figure, it is clear that second-order limiter MMs2 is relatively more oscillatory than others, but it has better shock resolution capability.
Cada limiter [39] has shown a better trade between shock resolution and over-shoots. Error of the test case is shown in Table 5. Though MMF1-S2 limiter has some over-shoots in the contact discontinuity than other limiters, it gives the least RMS error. The result of MMF1 is comparable to the second-order limiter. MMF1-S2 is 16% more accurate than Cada limiter.

6.2 Shu-Osher problem

The initial condition used is given in eq. (15). The problem is solved over the domain [-5, 5]. The simulation is carried up to flow time 1.8 s using 400 grid points. CFL number used is 0.5. MMF1 unable to resolve some peaks present in the solution. All the second-order limiters are outperformed by the third-order limiter MMF1-S2. The comparison of the different limiters is presented in Fig. 10. The reference solution is obtained using minmod limiter on 2000 grid points. The performance of Cada limiter and MMF1-S2 are good.

The RMS error of this problem is shown in Table 6. MMF1-S2 limiter is more accurate than other limiters and has the least RMS error. It is 53% and 20% more accurate than MMF1 limiter and Cada limiter respectively.

6.3 Blast waves interaction

In this test case, a low-pressure region is placed between two high-pressure regions on either side. The initial condition for this problem is:

$$(\rho, u, p) = \begin{cases} (1, 0, 1000) & x \geq 0 \quad and \quad x \leq 0.1 \\ (1, 0, 0.01) & x > 0.1 \quad and \quad x <= 0.9 \\ (1, 0, 1000) & x > 0.9 \quad and \quad x <= 1 \end{cases} \qquad (21)$$

This creates two blast waves moving towards the central low-pressure region and they intact with each other. When these waves meet each other, it produces high pressures. After that, they move outwards and the pressure at the centre reduces. This problem has a pressure ratio of 10^5 and the interacting blast wave can raise the pressure more than the thrice the initial pressure at the end of the shock tube. The solution is obtained by discretizing the domain [0, 1] with 400 grid point. The problem is solved up to 0.025 s. The reference solution is obtained using 2000 grid points. The solution is shown in Fig. 11. The L_2 error of this test case is shown in Table 7.

7. Conclusion

This paper discusses new second-order and third-order limiters. The shock resolution property and the limiter's accuracy are compared to other conventional limiters for standard benchmark problems. Flux extrapolation can be done either with the first derivative term alone or with both the first and the second derivatives (eq. (6)). Most of the limiters use higher-order first derivative information without considering the second-order gradient information. In this paper, second gradient terms are successfully incorporated in the limiter without oscillations. The present limiters are tested on the uniform and unstructured grid. The present limiters have shown a better shock resolving property and accuracy compared to other limiters. The performance of the present limiters on blast-wave problems is noteworthy, and it is 247% more accurate and 420% more accurate than the Cada limiter and Convex-ENO scheme. The method presented in this work is based on discretization. Because of the advancement of the computational power, similar equations could be solved with better accuracy using deep neural network [41] using global or non-gradient based optimization algorithms.

Author Contributions

The authors have an equal contribution to all the works carried in this report.

Conflict of Interest

The authors declared no potential conflicts of interest with respect to the research, authorship and publication of this article.

Data Availability Statements

The datasets generated and/or analyzed during the current study are available from the corresponding author on reasonable request.

Nomenclature

ρ	Density [kg/m³]		U	Velocity [m/s]
p	Pressure [N/m²]		E	Root mean square error
M	Mach number		CFL	Courant–Friedrichs–Lewy

References

[1] Zipay, J. J., Modlin, C. T., Larsen, C. E., The Ultimate Factor of Safety for Aircraft and Spacecraft-Its History, Applications and Misconceptions, *In 57th AIAA/ASCE/AHS/ASC Structures, Structural Dynamics, and Materials Conference*, 2016.

[2] Shao, Z., Riemann problem with delta initial data for the isentropic relativistic Chaplygin Euler equations, *Zeitschrift für Angewandte Mathematik und Physik*, 67(3), 2016, 66.

[3] Shao, Z., The Riemann problem for the relativistic full Euler system with generalized Chaplygin proper energy density–pressure relation, *Zeitschrift für Angewandte Mathematik und Physik*, 69(2), 2018, 44.

[4] Zhang, W., Wang, T., Bai, J. S., Li, P., Wan, Z. H., Sun, D. J., The piecewise parabolic method for Riemann problems in nonlinear elasticity, *Scientific Reports*, 7(1), 2017, 1-17.

[5] Jiang, G.S., Shu, C. W, Efficient implementation of weighted ENO schemes, *Journal of Computational Physics*, 126(1), 1996, 202-228.

[6] Appadu, A. R., Peer, A. A. I., Optimized weighted essentially non-oscillatory third-order schemes for hyperbolic conservation laws, *Journal of Applied Mathematics*, 2013, Article ID 428681.

[7] Zhang, D., Jiang, C., Liang, D., Cheng, L., A review on TVD schemes and a refined flux-limiter for steady-state calculations, *Journal of Computational Physics*, 302, 2015, 114-154.

[8] van Leer, B., Towards the ultimate conservative difference scheme. ii. monotonicity and conservation combined in a second-order scheme, *Journal of Computational Physics*, 14(4), 1974, 361-370.

[9] Hirsch, C., *Numerical computation of internal and external flows: The fundamentals of computational fluid dynamics*, Butterworth-Heinemann, 2007.

[10] Sweby, P. K., High Resolution Schemes Using Flux Limiters for Hyperbolic Conservation Laws, *SIAM Journal on Numerical Analysis*, 1984, 995-1011.

[11] Colella, P., Woodward, P. R., The Piecewise Parabolic Method (PPM) for gas-dynamical simulations, *Journal of Computational Physics*, 54(1), 1984, 174-201.

[12] Suresh, A., Huynh, H. T., Accurate monotonicity-preserving schemes with Runge-Kutta time stepping, *Journal of Computational Physics*, 136(1), 1997, 83-99.

[13] Marquina, A., Local Piecewise Hyperbolic Reconstruction of Numerical Fluxes for Nonlinear Scalar Conservation Laws, *SIAM J. ScI. Compt.*,15(4), 1994, 892-915.

[14] Waterson, N. P., Deconinck, H., Design principles for bounded higher-order convection schemes - a unified approach, *Journal of Computational Physics*, 244(1), 2007, 182-207.

[15] van Albada G. D., Leer, B. V., Roberts W. W., *A Comparative Study of Computational Methods in Cosmic Gas Dynamics*, Springer Berlin Heidelberg, Berlin, Heidelberg, 1997.

[16] Warming R. F., Beam R. M., Upwind Second-Order Difference Schemes and Applications in Aerodynamic Flows, *AIAA Journal*, 14(9), 1976, 1241-1249.

[17] Fromm, J. E., A method for reducing dispersion in convective difference schemes, *Journal of Computational Physics*, 3(2), 1968, 176-189.

[18] Agarwal R.K., A third-order-accurate upwind scheme for Navier-Stokes solutions at high Reynolds numbers, *19th Aerospace Science Meeting*, 1981.

[19] Leonard B. P., A stable and accurate convective modeling procedure based on quadratic upstream interpolation, *Computer Methods in Applied Mechanics and Engineering*, 19(1), 1979, 59-98.

[20] Roe, P. L., Baines, M. J., Algorithms for advection and shock problems, *Numerical Methods in Fluid Mechanics*, 1982, 281-290.

[21] Roe, P. L., Some contributions to the modelling of discontinuous flows, *Large-scale Computations in Fluid Mechanics*, 1985, 163-193.

[22] van Leer, B., Towards the ultimate conservative difference scheme. iv. a new approach to numerical convection, *Journal of Computational Physics*, 23(3), 1977, 276-299.

[23] van Albada G. D., van Leer, B., Roberts W. W., *A comparative study of computational methods in cosmic gas dynamics*, In: Hussaini M.Y., van Leer B., Van Rosendale J. (eds) Upwind and High-Resolution Schemes. Springer, Berlin, Heidelberg, 1997.

[24] Zhou, G., *Numerical simulations of physical discontinuities in single and multi-fluid flows for arbitrary Mach numbers*, Chalmers University of Technology, 1995.

[25] Ray, D., Chandrashekar, P., Fjordholm, U. S., Mishra, S., Entropy stable scheme on two-dimensional unstructured grids for Euler equations, *Communications in Computational Physics*, 19(5), 2016, 1111-1140.

[26] Koren, B., *A robust upwind discretization method for advection, diffusion and source terms*, Centrum voor Wiskunde en Informatica, Amsterdam, 1993.

[27] Chatkravathy, S. R., High resolution applications of the Osher upwind scheme for the Euler equations, AIAA paper 83-1943. In *Proc. AIAA 6th Computational Fluid Dynamics Conference*, 1983.

[28] Waterson, N.P., Deconinck, H., Design principles for bounded higher-order convection schemes-a unified approach, *Journal of Computational Physics*, 224(1), 2007, 182-207.

[29] Gaskell, P. H., Lau, A. K. C., Curvature-compensated convective transport: Smart, a new boundedness- preserving transport algorithm, *International Journal for Numerical Methods in Fluids*, 8(6), 1988, 617-641.

[30] Lien, F. S., Leschziner, M. A., Upstream monotonic interpolation for scalar transport with application to complex turbulent flows, *International Journal for Numerical Methods in Fluids*, 19(6), 1994, 527-548.

[31] Goodman, J. B., LeVeque, R. J., On the Accuracy of Stable Schemes for 2D Scalar Conservation Laws, *Mathematics of Computation*, 1985, 15-21.

[32] Kumar, R., Kadalbajoo, M. K., Efficient high-resolution relaxation schemes for hyperbolic systems of conservation laws, *International Journal for Numerical Methods in Fluids*, 55(5), 2007, 483-507.

[33] Kadalbajoo, M. K., Kumar, R., A high resolution total variation diminishing scheme for hyperbolic conservation law and related problems, *Applied Mathematics and Computation*, 175(2), 2006, 1556-1573.

[34] Kumar, R., Flux limited schemes: Their classification and accuracy based on total variation stability regions, *Applied Mathematics and Computation*, 224, 2013, 325-336.

[35] Kitamura, K., Roe, P. L., Ismail, F., An Evaluation of Euler Fluxes for Hypersonic Flow Computations, *AIAA Journal*, 47(1), 2007, 44-53.

[36] Neelan A. G., Nair, M. T., Hyperbolic Runge-Kutta method using Genetic Algorithm, *Journal of Computational and Nonlinear Dynamics*, 13(10), 2018, 101003.

[37] Masatsuka, K., *I do Like CFD*, Volume 1. Lulu.com, 2013.

[38] Liu, X. D., Osher, S., Convex ENO high order multi-dimensional schemes without field-by-field decomposition or staggered grids, *Journal of Computational Physics*, 142(2), 1998, 304–330.

[39] Cada, M., Torrilhon, M., Compact third-order limiter functions for finite volume methods, *Journal of Computational Physics*, 228(11), 2009, 4118-4145.

[40] Bryson A. E. Jr., An experimental investigation of transonic flow past two-dimensional wedge and circular-arc sections using a mach-zehnder interferometer, *NASA, Langley Research Center, Tech. Report*, 1952.

[41] Samaneiego, E., Anitescu, C., Goswami, S., Nguyen-Thanh, V. M., Guo, H., Hamdia, K., Rabczuk, T., An energy approach to the solution of partial differential equations in computational mechanics via machine learning: Concepts, implementation and applications, *Computer Methods in Applied Mechanics and Engineering*, 362, 2020, 112790.

ORCID iD

Arun Govind Neelan https://orcid.org/0000-0003-0882-0671

Manoj T. Nair https://orcid.org/0000-0001-6276-5170

Publisher's Note Shahid Chamran University of Ahvaz remains neutral with regard to jurisdictional claims in published maps and institutional affiliations.